

Article

# Laser Finishing of Ti6Al4V Additive Manufactured Parts by Electron Beam Melting

Silvio Genna <sup>1,2,\*</sup>  and Gianluca Rubino <sup>3</sup>

<sup>1</sup> Department of Enterprise Engineering Mario Lucertini, University of Rome Tor Vergata, Via del Politecnico 1, 00133 Rome, Italy

<sup>2</sup> CIRTIBS Research Centre, University of Naples Federico II, P.le Tecchio 80, 80125 Naples, Italy

<sup>3</sup> Department of Economics, Engineering, Society, and Business Organization, Università degli Studi della Tuscia, Via del Paradiso, 47, 01100 Viterbo, Italy; gianluca.rubino@unitus.it

\* Correspondence: silvio.genna@uniroma2.it

Received: 14 November 2019; Accepted: 22 December 2019; Published: 25 December 2019



**Abstract:** In this work, the feasibility of laser surface finishing of parts obtained by additive manufacturing (AM) was investigated. To this end, a 450 W fiber laser (operating in continuous wave, CW) was adopted to treat the surface of Ti-6Al-4V samples obtained via electron beam melting (EBM). During the tests, different laser energy densities and scanning speeds were used. In order to assess the quality of the treatment, either the as-built or the treated samples were analyzed by means of a three-dimensional (3D) profilometer, digital microscopy, and scanning electron microscopy. Analysis of variance (ANOVA) was performed to check which and how process parameters affected the finishing. The results show that, in the best conditions, the laser treatment reduced surface roughness by about 80%.

**Keywords:** EBM; surface roughness; microhardness; fiber laser

## 1. Introduction

Initially, three-dimensional (3D) printing was adopted just for rapid prototyping (RP); recently, it has been used as a real production technology, starting from the three-dimensional mathematical model, realized with CAD (computer aided design) software. The technique allows creating components by adding material “layer-by-layer”. This is the reason why it is also known as additive manufacturing (AM) [1]. By using different AM techniques, it is possible to obtain customized and complex components of different materials (metals, plastic or ceramic) with competitive costs and times [2]. In the aeronautic field, the most attractive materials are definitely metals, such as titanium and aluminum alloys, as they allow to design components with very complex shapes that are hardly obtained when using conventional technologies [2–4]. Metal parts can be obtained using different AM techniques and are all based on power bed fusion (PBF) technology [1], such as electron beam melting (EBM) [5], direct metal laser sintering (DMLS) [4,6], and selective laser melting (SLM) [7,8]. However, the surfaces of the printed parts all have a low quality. The typical arithmetic average of the roughness profile (Ra) varies in the range 8–25  $\mu\text{m}$  [2,6,9] depending on the adopted technology. Even if lower values of roughness are obtainable by laser sintering/melting, the EBM process is generally preferred for the production of aerospace components as it can produce high-quality products with excellent mechanical properties and fewer defects compared to those achieved by using laser technologies. Thus, it is possible to obtain almost fully-dense parts [3]. This is due to the EBM process: the parts are printed in a vacuum environment which eliminates all impurities with high build temperatures, and thus low residual stress. In addition, EBM has faster build rates and all elements do not necessarily require any support [9].

It is renowned that fatigue properties are strictly related to surface morphology; an increase in roughness leads to a reduction of fatigue life [10,11]. Nicoletto et al. [12] studied the influence of roughness and morphology on the fatigue life of Ti alloy components produced with different orientations, using either a laser or an EBM system. Thus, the finishing of the AM parts is an important issue; different techniques can be adopted, such as abrasive fluidized bed [2], laser treatment [13–16], and chemical polishing [17–19]. Laser treatments offer some advantages compared to the other aforementioned techniques, such as absence of any mechanical contact due to the lack of tools which lead to a no wear high accuracy and high repeatability. Laser treatments are ecofriendly since they do not use any solvent or chemical agent and work with different materials, such as metals, ceramic, and polymers, just by changing the wavelength. Ukar et al. [15] adopted a CO<sub>2</sub> laser to polish DIN 1.2379 tool steel, achieving a roughness reduction up to 90%. Gisario et al. [20] used a diode laser to modify the surface of bronze sintered parts. The main results were a 70% reduction in roughness and an increase in microhardness, scratch, and wear resistance. Chang et al. [21] adopted a pulsed fiber laser to polish a SKD61 steel tool, obtaining a reduction in roughness. Campanelli et al. [22] studied the laser finishing on parts obtained by SLM. A Taguchi methodology was adopted which identified the laser power, pulse frequency, and number of repetitions as the most affecting parameters.

The purpose of this work is to study the laser surface finishing of components (Ti-6Al-4V alloy) obtained by electron beam melting (EBM) by means of a high-efficiency fiber laser operating in continuous wave. The laser energy density and scanning speed were both varied during the tests. In order to assess the quality of the treatment, either the as-built or the treated samples were analyzed by means of a 3D profilometer, digital microscopy, and scanning electron microscopy. The results show that, in the best conditions, the laser treatment reduced surface roughness by about 80% and achieved a roughness Ra of about 5 µm.

## 2. Materials, Equipment, and Methods

### 2.1. Materials

The laser treatment was performed on the external surface of titanium alloy samples. The samples were built by the EBM technique (Arcam A2X), using gas-atomized Ti6Al4V ELI powders (particle size in the range of 45–100 µm) [23]. The main system characteristics are reported in Table 1. The samples were printed with a layer thickness of 50 µm. The chamber pressure before starting the process was  $5 \times 10^{-4}$  mbar; then helium gas was introduced into the chamber to avoid the smoke effect [3], and the pressure reached  $2 \times 10^{-3}$  mbar. During the process, a defocused beam of electrons pre-heated the laying powder (up to 750 °C), then a focused beam melted the powder according to a pattern achieved during the slicing phase.

**Table 1.** Arcam A2X characteristics. Abbreviations: CAD: computer aided design; STL: standard triangulation language.

Characteristics	Units	Value
Maximum build size	mm <sup>3</sup>	200 × 200 × 380
Beam power	W	3000
Cathode type	–	Tungsten filament
Min. beam diameter	µm	250
Max. EB translation speed	m/s	8000
Vacuum base pressure	mbar	$5 \times 10^{-4}$
Build atmosphere (partial pressure of He)	mbar	$2 \times 10^{-3}$
He consumption	l/h	1
CAD interface standard	–	STL

## 2.2. Laser Finishing Setup

A 450 W fiber laser (IPG YLR-450/4500-QCW-MM-AC-Y14) was used to finish the surface of the samples. The system can operate either in continuous wave (CW) or in a modulated wave known as “quasi continuous wave” (QCW). The laser radiation is transferred via 50  $\mu\text{m}$  core fiber, with a length of 5 m, to a collimator with a lens of 85 mm, mounted onto a micro cutting head (IPG FLC D 25) with a focusing lens of 100 mm. Thus, a beam diameter of about 60  $\mu\text{m}$  is achieved. The main laser source characteristics are reported in Table 2.

**Table 2.** Main laser characteristics. Abbreviations: YAG: yttrium aluminum garnet; CW: continuous wave; QCW: quasi continuous wave.

Characteristics	Units	Value
Source type	–	Yb-YAG
Wavelength	nm	1070
M <sup>2</sup> factor	–	5.87
Regime	–	CW/QCW
Maximal average power	W	450 (CW/QCW)
Maximal peak power	W	4500 (in QCW)
Pulse duration	ms	0.05–50 ms (in QCW)
Focal length	mm	100
Declared focal spot	$\mu\text{m}$	$\approx 60$

During all tests, the CW mode was adopted in order to achieve a smoother surface. Nitrogen gas with a flow rate of 12 l/min at 2 bar was adopted to shield the samples, thus avoiding oxidation. The samples were rotated using a stepping motor (SANYODENKI 103H7126) at 200 rpm, while the laser was switched on outside the sample. The laser beam was then moved onto the samples at different speeds, with a length of about 50 mm, as reported in Figure 1. After the laser treatment, the samples were sandblasted with pink corundum (mesh size 120) at a pressure of 4 bar, with the aim to remove any incoherent material, and then cleaned in an ultrasonic bath with acetone to remove any traces of sand.

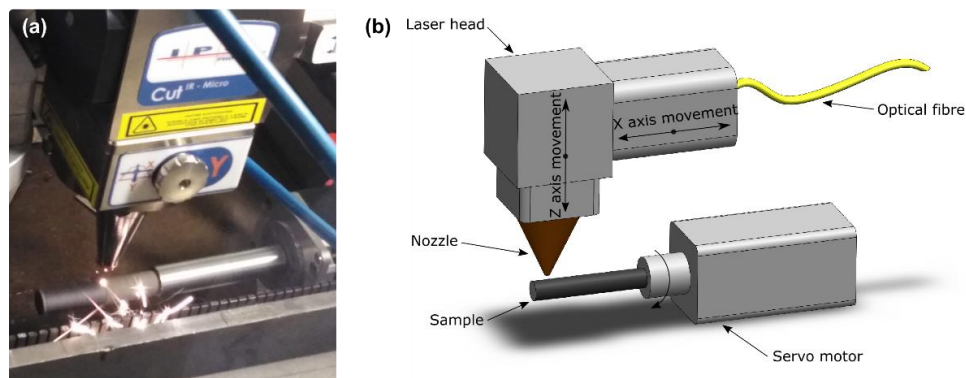


**Figure 1.** Experimental setup for laser finishing: (a) real image; (b) schematic view.

## 2.3. Experimental Procedures

The work was divided into two phases. In the first phase, preliminary tests were performed aimed at identifying the laser parameters (i.e., the control factors) to allow the treatment (i.e., the process windows) and the levels adopted in the second phase in which a  $2 \times 3$  factorial plan was defined and tested.

It is known that the laser energy density (i.e., the so called fluence) affects the interaction between laser and material. When the density increases, it is possible to pass from heating up to melting or even vaporizing the material. In other words, the fluence affects the amount of treated surface, the final roughness, and the heat affected zone (HAZ). The adopted solution to decrease the energy density is to vary the focal distance. At the increase of the focal distance, an increase of the laser footprint/track on the surface of the specimens occurs, and accordingly, a decrease of the fluence.

Preliminary tests were carried out keeping the laser radiation on the samples at maximum power (i.e., 450 W) with three different focal distances (+5, +7.5, and +10 mm) on the surface of the samples during rotation.

In the second phase, a  $2 \times 3$  factorial plan was defined and tested based on the results of the first phase. Table 3 shows the control factors and their levels. The plan was repeated three times; thus, a total of 18 tests were performed. The influence of the process parameters on the roughness of the samples was assessed via analysis of variance (ANOVA). The main effect and the interaction plots were plotted to see the effect of the control factors on the laser finishing.

**Table 3.** Control factors and their levels.

Control Factors	Labels	Low (–)	Middle (0)	High (+)	Unit
Scan speed	Ss	3.6	9	18	mm/min
Focal distance	Fd	5	–	7.5	mm

In order to assess the quality of the treatment, the surface morphology of as-built and treated samples were studied by means of a digital microscope (Hirox KH 8700). In addition, roughness measurements were performed on all samples using a 3D surface profiling system (Taylor Hobson Talysurf CLI 2000). More specifically, in order to characterize the surface topography [24], the amplitude roughness parameters were calculated on the acquired profile: the arithmetic mean surface roughness ( $R_a$ ) and the root mean squared surface roughness ( $R_z$ ), skewness ( $R_{sk}$ ), and kurtosis ( $R_{ku}$ ) were calculated in height; the mean width of profile elements ( $R_{Sm}$ ) was calculated horizontally. In addition, the root mean square slope ( $RDq$ ), defined as a hybrid parameter (i.e., a combination of amplitude and spacing), was calculated. The latter parameter was studied as it is known to influence tribological properties.

For what concerns roughness analysis, the cut-off and evaluation length were chosen as foreseen by the UNI EN ISO 4288:2000 standard reported in Table 4. Accordingly, for the as-built sample, the cut-off was set at 8, while for the finished samples, when  $R_a$  was in the range 2–10  $\mu\text{m}$ , it was set at 2.5. In addition, 3D maps of  $4 \times 4 \text{ mm}^2$  areas of the samples were also acquired using a resolution of 2  $\mu\text{m}$  along both directions.

**Table 4.** Recommended cut-off and evaluation length according to the UNI EN ISO 4288:2000 standard.

Profile		Cutoff	Evaluation Length
$R_z$ ( $\mu\text{m}$ )	$R_a$ ( $\mu\text{m}$ )	$\lambda$ (mm)	$l_n$ (mm)
Up to 0.1	Up to 0.02	0.08	0.4
0.1–0.5	0.02–1	0.25	1.25
0.5–10	1–2	0.8	4
10–50	2–10	2.5	12.5
50–200	10–80	8	40

After the acquisitions, the samples were cut with a diamond saw, embedded in an epoxy resin and polished. Then, micro-indentation tests (CSM Instruments Micro-Combi) were performed on the cross-sections, using a load of 20 N, starting at 0.75 mm from the edge up to the center of the samples with a step of 0.2 mm. Then, a chemical etching was performed in HF solution to analyze the microstructure of the specimens in order to assess the effect of the laser treatments.

### 3. Results

#### 3.1. Preliminary Tests

Figure 2 depicts the preliminary results of the samples treated with three different fluences, by way of focal distance: +5, +7.5, and +10 mm on the surface of the samples. Three different states are visible:

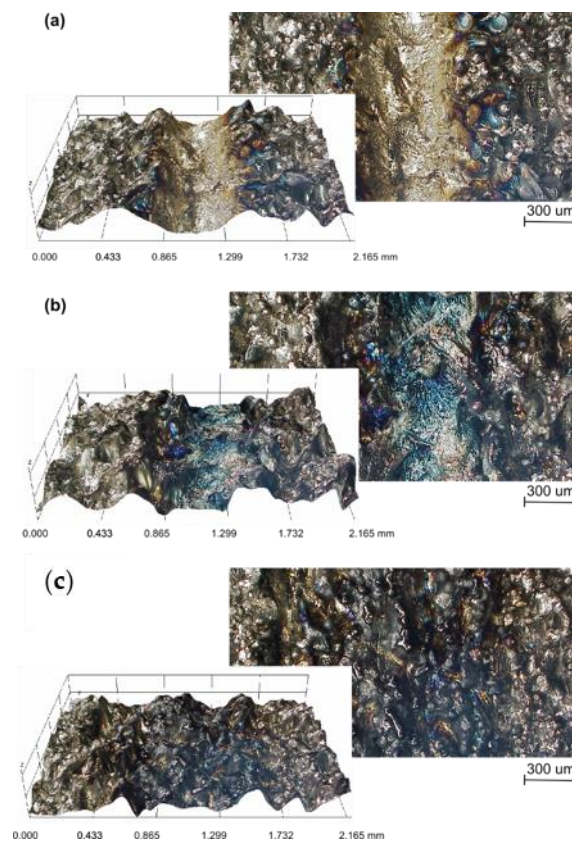


**Figure 2.** Laser tracks on the surfaces of specimens performed at: (a)  $Fd = 5$  mm, (b)  $Fd = 7.5$  mm, (c)  $Fd = 10$  mm.

a-state—the laser track appears regular with the typical V-shape of a deep marking. This means that the adopted fluence is so high as to vaporize the little ridges and part of the bulk (Figure 2a).

b-state—the laser track is just visible. The fluence is high enough to melt and vaporize only the little ridges while the bulk is light blue (Figure 2b).

c-state—the laser track is not visible. Just a dark shade is visible on the ridges and no melted material (Figure 2c).

According to these observations, the c-state was not desired for finishing purposes; consequently, focal distance ( $Fd$ ) = 10 mm was excluded from the second phase.

The screening tests show that, as expected, the fluence affects the interaction between the laser and material. When the density increases, it is possible to pass from heating up to melting or even vaporizing the material. If we consider the tracks, laser power, and treatment time, we can achieve an estimation of the adopted fluences. It is worth noting that these values differ from the theoretical ones but are more suitable for industrial applications. The measurements are reported in Table 5, while in Figure 3 the contour plot of the estimated fluence was traced vs. the track width and focal distance.

**Table 5.** Width of laser tracks at different focal distances.

Focal Distance, $Fd$ (mm)	Track Width, $Tw$ (mm)
5	0.57
7.5	0.74
10	1.04

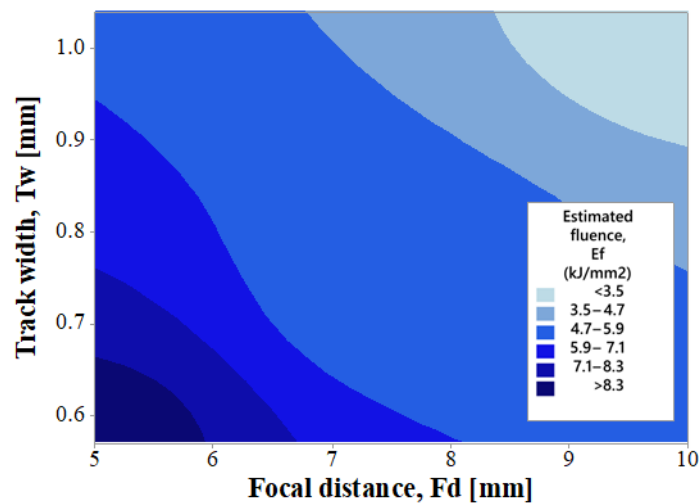


Figure 3. Contour plot of estimated fluence vs. track width and focal distance.

### 3.2. Morphological Analysis

Figure 4 shows the surface morphology of an as-built sample. As expected, the surface appears very irregular, with high peaks and valleys very close to one other. This is due to the melting of the smaller powder particles near the surface of the component, as observable in Figure 5a,b reporting respectively the cross-section surface and its magnification. From the analysis of the cross-section, it clearly appears that the outline is very jagged and the profilometer inductive stylus, with a 2  $\mu\text{m}$  radius, cannot penetrate in the very narrow valleys. Thus, the roughness parameters calculated on the acquired profiles of the as-built surface may be underestimated.

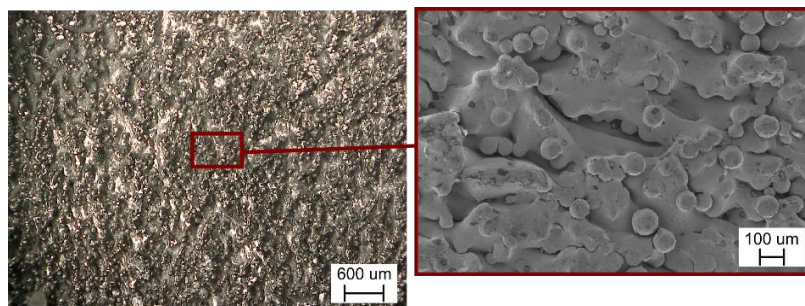


Figure 4. Surface morphology of an as-built sample.

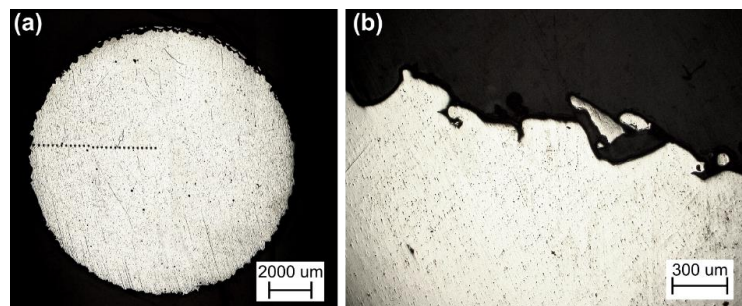
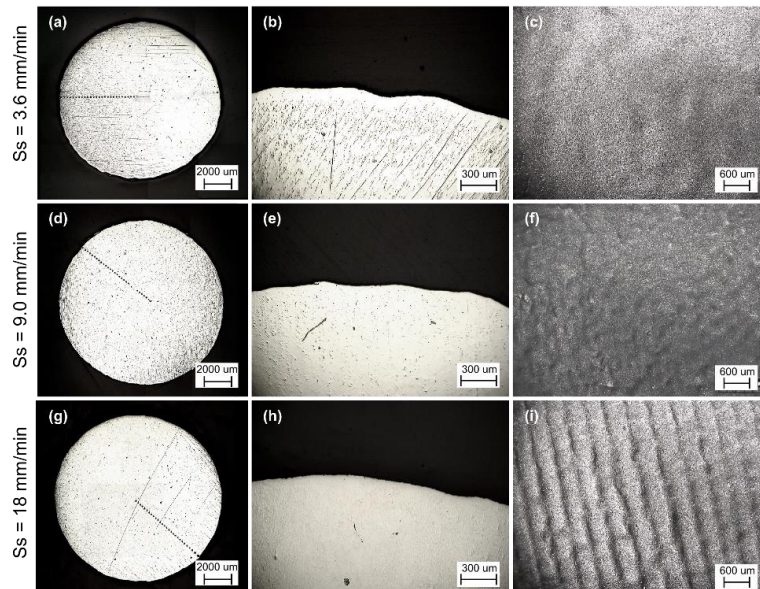


Figure 5. (a) Cross-section of as-built sample; (b) magnification of the external surface.

Figures 6 and 7 depict the cross-sections with their magnifications and the surface morphologies of laser-treated surfaces performed at  $Fd = 5\text{ mm}$  and  $Fd = 7.5\text{ mm}$ , respectively. As shown, the surfaces appear very different from the as-built one; the profile of the cross-sections appears smoother, while the peaks seem lower. Three different morphologies can be observed on the external surfaces:

Type 1: The surface appears smooth (Figure 6c), no laser track and ridges are visible;  
 Type 2: Some little ridges are visible (Figures 6f and 7c,f,i);  
 Type 3: Visible laser melting tracks (Figure 6i).



**Figure 6.** (a,d,g) Cross-sections, (b,e,h) their magnifications, and (c,f,i) surface morphologies after laser polishing at different Ss and Fd = 5 mm.

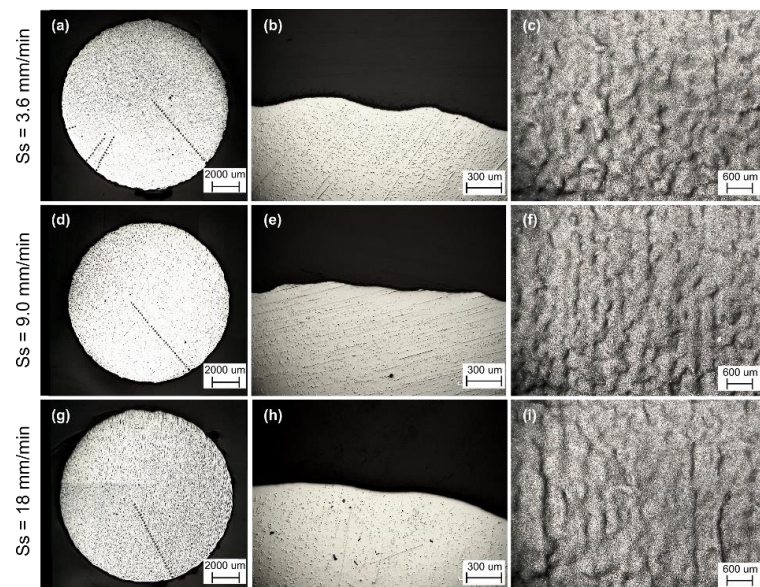


**Figure 7.** (a,d,g) Cross-sections, (b,e,h) their magnifications, and (c,f,i) surface morphologies after laser polishing at different Ss and Fd = 7.5 mm.

These morphologies are the consequence of the laser spot, rotating, and scan speed. A value that considers these parameters is the circumferential overlap percentage (COP) [25], which is defined as the following ratio:

$$COP = 1 - \frac{60 \times Ss}{D \times N} \tag{1}$$

where  $N$ ,  $D$ , and  $Ss$  represent the workpiece rotating speed in rpm, the laser spot in mm, and the scan speed in mm/s.

Then, based on the preliminary results of Table 5, it is possible to calculate the COP for each test condition by replacing the laser footprint at different focal distances (the values are reported in Table 6). The results show that at the minimum focal distance, the COP is in the range 84%–97%. However, in Figure 6i the laser tracks are visible. This is due to the Gaussian shape of the beam: the central part of the laser beam results in material vaporization, while the tails just allow the melting. This effect is not visible in Figure 6c,d because of the low scan speed (i.e., very high COP).

**Table 6.** Circumferential overlap percentage (COP) at different scan speed and focal distance.

Ss (mm/min)	Circumferential Overlap Percentage (%)	
	Fd = 5 mm	Fd = 7.5 mm
3.6	97	98
9	92	94
18	84	88

To better understand the phenomena occurring during the laser finishing, the treated surfaces were also analyzed by scanning electron microscopy (SEM). Figure 8 depicts the SEM images of the surface after laser polishing at different scan speed (Ss) and Fd. From the image, the lower focal distance (Fd = 5 mm) allows obtaining the smoothest surfaces by vaporizing the higher peaks and melting the greater ones. On the contrary, at a higher focal distance (Fd = 7.5 mm), the higher peaks are just melted and thus the surface appears more irregular. Consequently, at a lower focal distance, a higher diameter reduction of the sample is expected. In Figure 9, the sample’s diameter and its ablation are reported vs. the laser parameters. The figure represents a confirmation of the aforementioned mechanism (i.e., higher ablation at Fd = 5 mm).

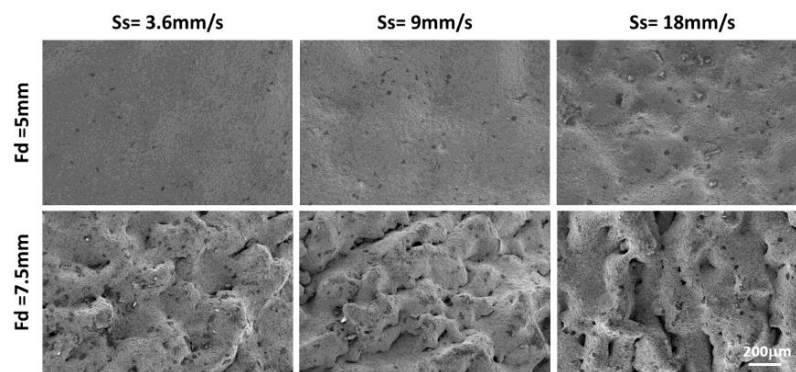


**Figure 8.** Scanning electron microscopy (SEM) images of the surface after laser polishing at different Ss and Fd.

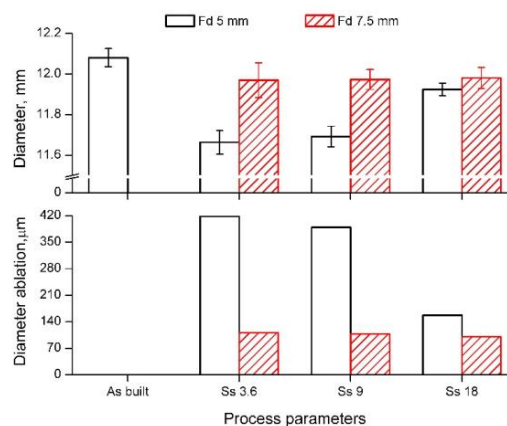


**Figure 9.** Samples diameter and diameter ablation vs. laser parameters.

### 3.3. Surface Roughness

Figures 10 and 11 depict the comparison of 3D maps and surface profiles acquired by the profilometer respectively on the as-built and on the laser-polished samples. The analysis confirms the smoother surface when the lower focal distance was adopted ( $Fd = 5\text{ mm}$ ). In order to better analyze the improvement, all the acquired roughness parameters are reported in Figure 12 vs. the laser ones. For the as-built samples, an arithmetic mean surface roughness ( $Ra$ ) of about  $27\text{ }\mu\text{m}$  is observable; while for the treated sample, in the best conditions, a  $Ra$  value of about  $5\text{ }\mu\text{m}$  can be obtained, allowing an 80% reduction in the roughness surface.

ANOVA was performed to assess the influence of the process parameters on sample roughness; the residual distribution was previously checked and a confidence level of 95% was adopted ( $\alpha = 0.05$ ). The results for  $Ra$  are reported in Table 7, where the model summary is also reported in terms of  $R^2$ . It is worth noting that the  $R^2$  value is very high, this means that the model has a good fit; the predicted  $R^2$  is high, thus the model has a good predictive ability. Based on these assumptions, both the control factors ( $Fd$  and  $Ss$ ) and their interaction are significant (i.e.,  $p$ -value less than 0.05). However, the most affecting factor is surely the focal distance ( $Fd$ ), since it shows the greatest  $F$ -value. Figure 13 depicts the main effect plot and interaction plot for  $Ra$ . Figure 13a shows that the effect of the control factors (i.e., the laser parameters). The roughness increases when the focal distance and scan speed increases (i.e., when energy density and laser–material interaction decrease); this result is consistent in literature. The effect of the interaction between the focal distance and scan speed can be seen in Figure 13b: at  $Fd = 7.5\text{ mm}$  the roughness parameter is not affected by a significant variation, while at  $Fd = 5\text{ mm}$ ,  $Ra$  changes from 5 up to 20. This aspect can be clarified by considering the surface morphologies of Figures 6 and 7.

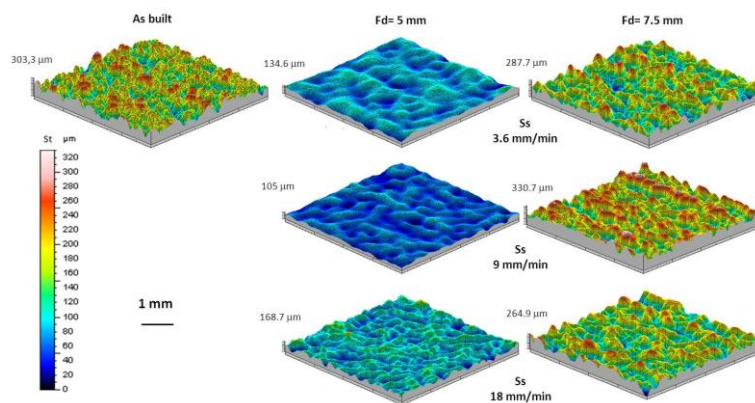


Figure 10. Roughness analysis: three-dimensional (3D) maps of the as-built and treated samples.

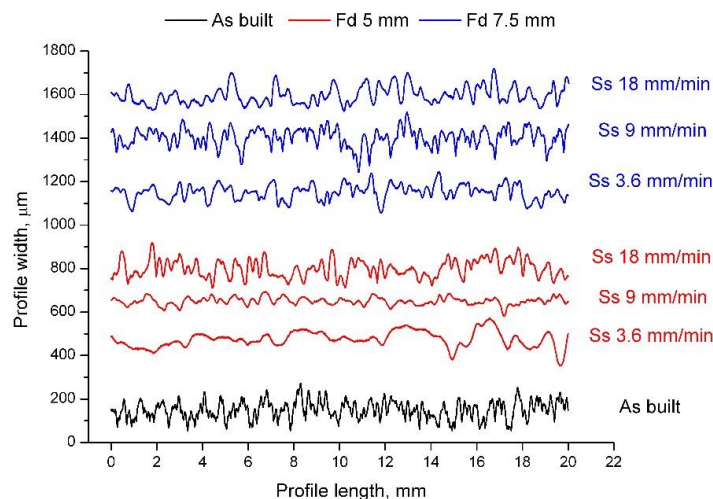


Figure 11. Surface profiles of as-built and treated samples.

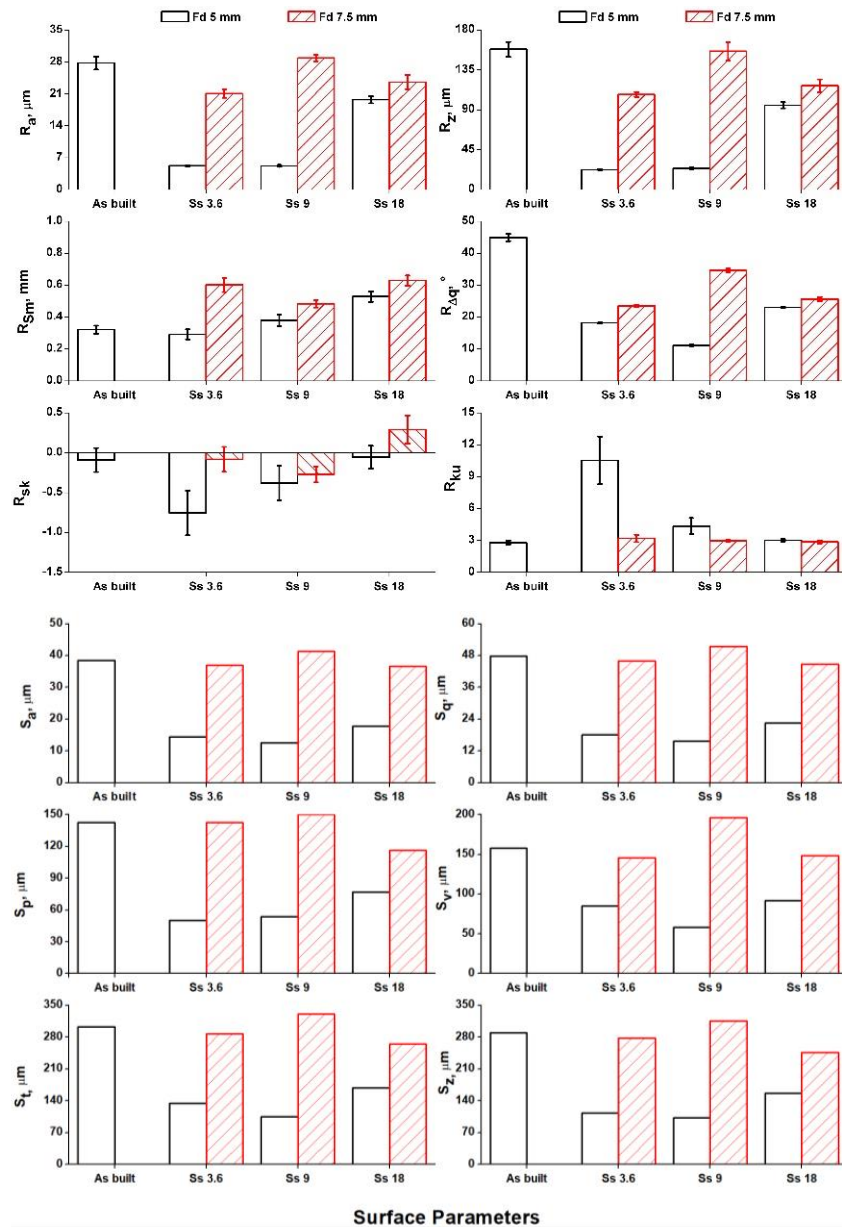


Figure 12. Roughness parameters vs. laser parameters.

Table 7. Analysis of variance results for Ra.

Source	DF	Adj SS	Adj MS	F-Value	p-Value
Fd (mm)	1	623.46	623.463	142.26	0.000
Ss (mm/min)	2	149.35	74.673	17.04	0.003
Fd (mm) × Ss (mm/min)	2	194.40	97.199	22.18	0.002
Error	6	26.29	4.382		
Total	11	993.50			

Model Summary	$R^2$	$R^2$ (adj)	$R^2$ (pred)
	97.35%	95.15%	89.41%

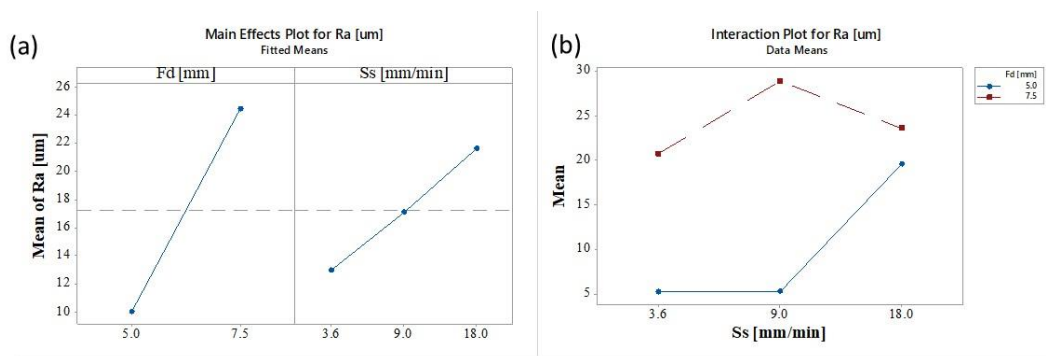


Figure 13. (a) Main effect plot and (b) interaction plot for Ra.

### 3.4. Microhardness Analysis

Figure 14 shows microhardness distribution along the cross-sections. No trend with edge distance is visible (about 330 HV for all samples, including the as-built one). As can be inferred, this outcome was not expected since laser treatment is a thermal interaction and therefore generally affects mechanical characteristics [13,16]. Then, a chemical etching was performed to analyze the microstructure of the specimens. In Figure 15 the microstructure analysis of an as-built and a laser-polished sample (Fd = 5 mm, Ss = 3.6 mm/min) are reported: the as-built sample shows the typical microstructure of Ti alloy (lamellar  $\alpha + \beta$  phase); the laser finished sample shows a polished layer (HAZ, heat affected zone) with a thickness of about 25  $\mu\text{m}$ . This is consistent [16,26,27] and related to melting and rapid cooling during laser finishing. It also explains the distribution of the microhardness distribution: the polished layer is too thin to allow a microhardness test (starting at 0.75 mm from the edge). Probably, a nanoindentation test would allow a measurement of the change in mechanical characteristics.

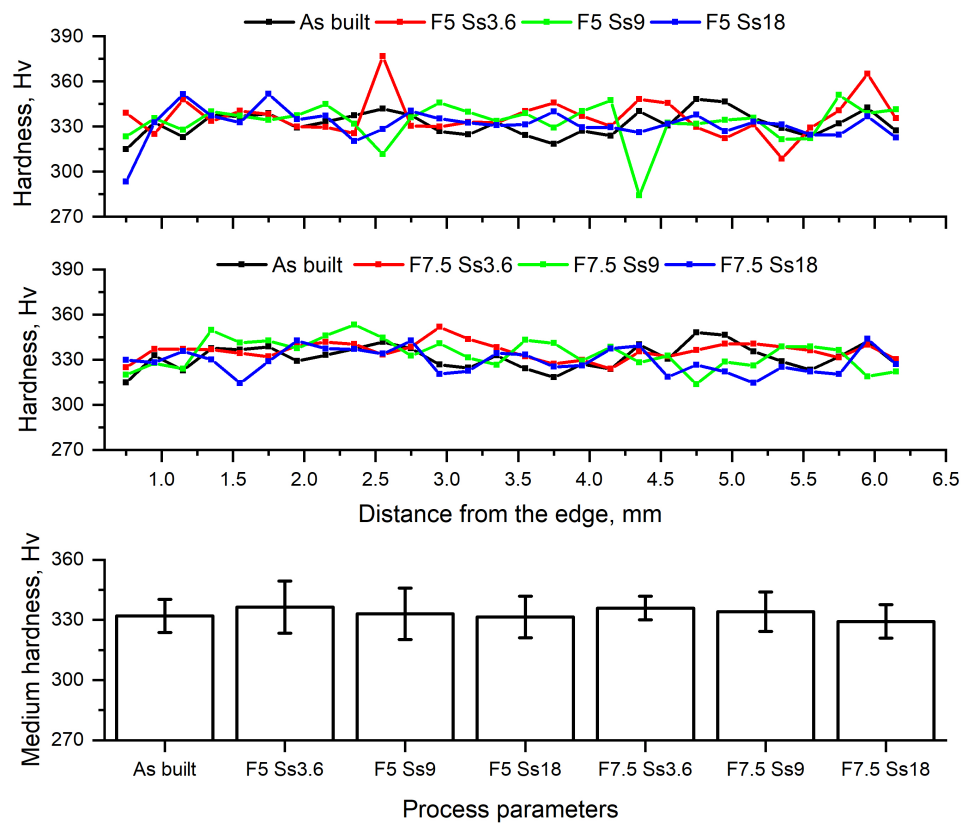
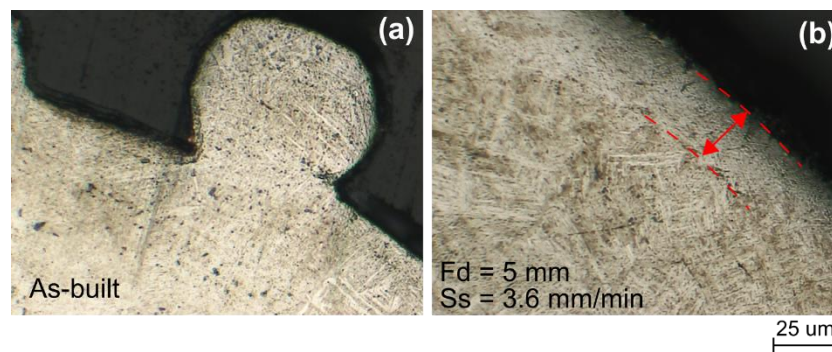


Figure 14. Microhardness along the cross section.



**Figure 15.** Microstructure analysis of (a) as-built and (b) laser-polished samples.

#### 4. Conclusions

In this paper, laser surface finishing of components obtained by electron beam melting (EBM) was performed. A high-efficiency fiber laser operating in continuous wave was used to treat the surface of Ti-6Al-4V samples. During the tests, the laser energy density (by way of focal distance) and the scanning speed were varied. The following findings were found:

The laser treatment can be adopted as a polishing treatment of Ti-6Al-4V samples. In the best conditions, a Ra value of about 5  $\mu\text{m}$  can be obtained with a reduction of 80% in roughness.

The main mechanism consists of melting and/or vaporization (depending on the laser energy) of the highest peaks.

The treatment involves material ablation and, therefore, the increase in dimensions must be considered when the components are designed.

The polished thickness (HAZ) is very small (about 25  $\mu\text{m}$  at Fd = 5 mm, Ss = 3.6 mm/min).

**Author Contributions:** All the authors contributed equally to the various aspect of this work. All authors have read and agreed to the published version of the manuscript.

**Funding:** This research received no external funding.

**Conflicts of Interest:** The authors declare no conflict of interest.

#### References

1. Bandyopadhyay, A.; Bose, S. *Additive Manufacturing*; CRC Press: Boca Raton, FL, USA, 2016.
2. Atzeni, E.; Barletta, M.; Calignano, F.; Iuliano, L.; Rubino, G.; Tagliaferri, V. Abrasive Fluidized Bed (AFB) finishing of AlSi10Mg substrates manufactured by Direct Metal Laser Sintering (DMLS). *Addit. Manuf.* **2016**, *10*, 15–23. [[CrossRef](#)]
3. Zhang, L.-C.; Liu, Y.; Li, S.; Hao, Y. Additive Manufacturing of Titanium Alloys by Electron Beam Melting: A Review. *Adv. Eng. Mater.* **2018**, *20*, 1700842. [[CrossRef](#)]
4. Manfredi, D.; Calignano, F.; Ambrosio, E.P.; Krishnan, M.; Canali, R.; Biamino, S.; Pavese, M.; Atzeni, E.; Iuliano, L.; Fino, P.; et al. Direct Metal Laser Sintering: An additive manufacturing technology ready to produce lightweight structural parts for robotic applications. *Metall. Ital.* **2013**, *105*, 15–24.
5. Chern, A.H.; Nandwana, P.; Yuan, T.; Kirka, M.M.; Dehoff, R.R.; Liaw, P.K.; Duty, C.E. A review on the fatigue behavior of Ti-6Al-4V fabricated by electron beam melting additive manufacturing. *Int. J. Fatigue* **2019**, *119*, 173–184. [[CrossRef](#)]
6. Khaing, M.; Fuh, J.Y.; Lu, L. Direct metal laser sintering for rapid tooling: Processing and characterisation of EOS parts. *J. Mater. Process. Technol.* **2001**, *113*, 269–272. [[CrossRef](#)]
7. Thijs, L.; Verhaeghe, F.; Craeghs, T.; Van Humbeeck, J.; Kruth, J.-P. A study of the microstructural evolution during selective laser melting of Ti-6Al-4V. *Acta Mater.* **2010**, *58*, 3303–3312. [[CrossRef](#)]
8. Wycisk, E.; Emmelmann, C.; Siddique, S.; Walther, F. High Cycle Fatigue (HCF) Performance of Ti-6Al-4V Alloy Processed by Selective Laser Melting. *Adv. Mater. Res.* **2013**, *816*, 134–139. [[CrossRef](#)]

9. Ahmed, N.; Abdo, B.M.; Darwish, S.; Moiduddin, K.; Pervaiz, S.; AlAhmari, A.M.; Naveed, M. Electron beam melting of titanium alloy and surface finish improvement through rotary ultrasonic machining. *Int. J. Adv. Manuf. Technol.* **2017**, *92*, 3349–3361. [[CrossRef](#)]
10. Greitemeier, D.; Donne, C.D.; Syassen, F.; Eufinger, J.; Melz, T. Effect of surface roughness on fatigue performance of additive manufactured Ti–6Al–4V. *Mater. Sci. Technol.* **2016**, *32*, 629–634. [[CrossRef](#)]
11. Bagehorn, S.; Wehr, J.; Maier, H. Application of mechanical surface finishing processes for roughness reduction and fatigue improvement of additively manufactured Ti–6Al–4V parts. *Int. J. Fatigue* **2017**, *102*, 135–142. [[CrossRef](#)]
12. Nicoletto, G.; Konečná, R.; Frkáň, M.; Riva, E. Surface roughness and directional fatigue behavior of as-built EBM and DMLS Ti6Al4V. *Int. J. Fatigue* **2018**, *116*, 140–148. [[CrossRef](#)]
13. Lamikiz, A.; Sanchez, J.A.; De Lacalle, L.L.; Arana, J.; Mentxaka, A.L.; De Lacalle, L.N.L. Laser polishing of parts built up by selective laser sintering. *Int. J. Mach. Tools Manuf.* **2007**, *47*, 2040–2050. [[CrossRef](#)]
14. Temmler, A.; Willenborg, E.; Wissenbach, K. Laser Polishing. *SPIE LASE* **2012**, *8243*, 82430.
15. Ukar, E.; Lamikiz, A.; De Lacalle, L.L.; Del Pozo, D.; Arana, J.; Mentxaka, A.L.; De Lacalle, L.N.L. Laser polishing of tool steel with CO<sub>2</sub> laser and high-power diode laser. *Int. J. Mach. Tools Manuf.* **2010**, *50*, 115–125. [[CrossRef](#)]
16. Ma, C.; Guan, Y.; Zhou, W. Laser polishing of additive manufactured Ti alloys. *Opt. Lasers Eng.* **2017**, *93*, 171–177. [[CrossRef](#)]
17. Scherillo, F. Chemical surface finishing of AlSi10Mg components made by additive manufacturing. *Manuf. Lett.* **2019**, *19*, 5–9. [[CrossRef](#)]
18. Tyagi, P.; Goulet, T.; Riso, C.; Garcia-Moreno, F. Reducing surface roughness by chemical polishing of additively manufactured 3D printed 316 stainless steel components. *Int. J. Adv. Manuf. Technol.* **2019**, *100*, 2895–2900. [[CrossRef](#)]
19. Gora, W.S.; Tian, Y.; Cabo, A.P.; Ardron, M.; Maier, R.R.; Prangnell, P.; Weston, N.J.; Hand, D.P. Enhancing Surface Finish of Additively Manufactured Titanium and Cobalt Chrome Elements Using Laser Based Finishing. *Phys. Procedia* **2016**, *83*, 258–263. [[CrossRef](#)]
20. Gisario, A.; Barletta, M.; Veniali, F. Surface reconstruction of porous substrates in sintered bronze by cw-high power diode laser. *Opt. Lasers Eng.* **2012**, *50*, 1306–1315. [[CrossRef](#)]
21. Chang, C.-S.; Chen, T.-H.; Li, T.-C.; Lin, S.-L.; Liu, S.-H.; Lin, J.-F. Influence of laser beam fluence on surface quality, microstructure, mechanical properties, and tribological results for laser polishing of SKD61 tool steel. *J. Mater. Process. Technol.* **2016**, *229*, 22–35. [[CrossRef](#)]
22. Campanelli, S.; Casalino, G.; Contuzzi, N.; Ludovico, A. Taguchi Optimization of the Surface Finish Obtained by Laser Ablation on Selective Laser Molten Steel Parts. *Procedia CIRP* **2013**, *12*, 462–467. [[CrossRef](#)]
23. Ti6Al4V ELI Titanium Alloy Arcam EBM System. Available online: [www.arcam.com](http://www.arcam.com) (accessed on 17 July 2019).
24. Gadelmawla, E.; Koura, M.; Maksoud, T.; Elewa, I.; Soliman, H. Roughness parameters. *J. Mater. Process. Technol.* **2002**, *123*, 133–145. [[CrossRef](#)]
25. Kibria, G.; Lepcha, L.P.; Shivakoti, I.; Doloi, B.; Bhattacharyya, B. Pulsed Nd:YAG Laser Micro-turning of Alumina to Study the Effect of Overlap Factors on Surface Roughness Performance. *IOP Conf. Ser. Mater. Sci. Eng.* **2018**, *377*, 012185. [[CrossRef](#)]
26. Wu, S.; Lu, Y.; Gan, Y.; Huang, T.; Zhao, C.; Lin, J.; Guo, S.; Lin, J. Microstructural evolution and microhardness of a selective-laser-melted Ti–6Al–4V alloy after post heat treatments. *J. Alloys Compd.* **2016**, *672*, 643–652. [[CrossRef](#)]
27. Hahn, J.D.; Shin, Y.C.; Krane, M.J.M. Laser transformation hardening of Ti–6Al–4V in solid state with accompanying kinetic model. *Surf. Eng.* **2007**, *23*, 78–82. [[CrossRef](#)]

